Magn Reson Mater Phy (2016) 29:399–415
DOI 10.1007/s10334-016-0541-8

RESEARCH ARTICLE

The traveling heads: multicenter brain imaging at 7 Tesla

Maximilian N. Voelker[1] · Oliver Kraff[1] · Daniel Brenner[2] · Astrid Wollrab[3] · Oliver Weinberger[4] · Moritz C. Berger[5] · Simon Robinson[6] · Wolfgang Bogner[6] · Christopher Wiggins[7] · Robert Trampel[8] · Tony Stöcker[2] · Thoralf Niendorf[4,9] · Harald H. Quick[1,10] · David G. Norris[1,11] · Mark E. Ladd[1,5] · Oliver Speck[3,12,13,14]

Received: 9 December 2015 / Revised: 8 February 2016 / Accepted: 25 February 2016 / Published online: 20 April 2016

Abstract
Objective This study evaluates the inter-site and intra-site reproducibility of 7 Tesla brain imaging and compares it to literature values for other field strengths.
Materials and methods The same two subjects were imaged at eight different 7 T sites. MP2RAGE, TSE, TOF, SWI, EPI as well as B1 and B0 field maps were analyzed quantitatively to assess inter-site reproducibility. Intra-site reproducibility was measured with rescans at three sites.
Results Quantitative measures of MP2RAGE scans showed high agreement. Inter-site and intra-site reproducibility errors were comparable to 1.5 and 3 T. Other sequences also showed high reproducibility between the sites, but differences were also revealed. The different RF coils used were the main source for systematic differences between the sites.
Conclusion Our results show for the first time that multicenter brain imaging studies of the supratentorial brain can be performed at 7 T with high reproducibility and similar reliability as at 3T. This study develops the basis for future large-scale 7 T multi-site studies.

Keywords Magnetic resonance imaging · Neuroimaging · Ultrahigh field · Multi-center

Introduction

The number of ultrahigh field (UHF) magnetic resonance (MR) system installations continues to increase, with currently approximately 70 research sites in operation worldwide. As a main advantage, this new technology provides

✉ Maximilian N. Voelker
Maximilian.Voelker@uni-due.de

[1] Erwin L. Hahn Institute for Magnetic Resonance Imaging, University of Duisburg-Essen, Kokereiallee 7, 45141 Essen, Germany

[2] German Center for Neurodegenerative Diseases (DZNE), Bonn, Germany

[3] Department of Biomedical Magnetic Resonance, Otto-von-Guericke-University Magdeburg, Magdeburg, Germany

[4] Berlin Ultrahigh Field Facility (B.U.F.F.), Max-Delbrueck-Center for Molecular Medicine, Berlin, Germany

[5] Medical Physics in Radiology, German Cancer Research Center (dkfz), Heidelberg, Germany

[6] Department of Biomedical Imaging and Image-guided Therapy, High Field MR Center, Medical University of Vienna, Vienna, Austria

[7] Scannexus, Maastricht, Netherlands

[8] Max Planck Institute for Human Cognitive and Brain Sciences, Leipzig, Germany

[9] Experimental and Clinical Research Center, A Joint Cooperation Between the Charité Medical Faculty and the Max Delbrück Center for Molecular Medicine, Berlin, Germany

[10] High Field and Hybrid MR Imaging, University Hospital Essen, University Duisburg-Essen, Essen, Germany

[11] Donders Centre for Cognitive Neuroimaging, Nijmegen, Netherlands

[12] Leibniz Institute for Neurobiology, Magdeburg, Germany

[13] German Center for Neurodegenerative Disease (DZNE), Magdeburg, Germany

[14] Center for Behavioral Brain Sciences, Magdeburg, Germany

a higher signal-to-noise ratio (SNR) and sensitivity [1], yet the artifact-to-noise ratio [2] can also be increased. This can degrade image quality and may differ at individual UHF sites, where system hardware differences could affect reproducibility. In UHF brain imaging, inhomogeneities due to wavelength effects are less pronounced than in body or cardiac imaging because of smaller object size relative to the radiofrequency (RF) wavelength [3]. Image quality and reproducibility, however, may still be compromised due to such RF effects. With increasing maturity of UHF MR, many studies have showed that brain imaging is one of the most beneficial applications at 7 T and clinical research is starting to exploit UHF advantages [4]. The next step is clinical approval of 7 T MRI for brain imaging and also musculoskeletal imaging, as currently announced by one manufacturer [5].

Inter-site reproducibility is not only a requirement for UHF application in clinical diagnosis but also for larger multicenter trials and quantitative data analysis. Such reproducibility has previously been established at 3 T [6] for multicenter studies of neurological diseases, i.e., Alzheimer's disease [7–9], to reliably detect and quantify changes in brain volume, grey and white matter compartments, or cortical and subcortical structures (like hippocampus, cerebellum, etc).

The higher spatial resolution and sensitivity of 7 T may allow extension of previous 3 T group study results to single subject level in longitudinal studies and also open the possibility for 7 T multi-site studies. However, inter-site reproducibility has not yet been investigated for 7 T brain imaging. A recent study [10] showed the potential advantage of 7 T over 3 T for high-resolution Voxel-based morphometry (VBM) mapping, but noted that statistical methods are sensitive to image inhomogeneities. Other quantitative measures, such as cortical thickness, also benefit from the high spatial resolution achievable with 7 T, but reproducibility across sites needs to be demonstrated [11].

To establish the consistency and reproducibility of quantitative measures between 7 T systems, the "traveling heads" experiment was initiated in 2014 to compare human brain imaging at a number of 7 T installations [12]. A 7 T brain imaging protocol with state-of-the-art UHF sequences was applied and image quality compared between eight different 7 T MRI sites of the same vendor. To separate site and system differences from inter-subject variations, the same two "traveling heads" were imaged at all sites.

Materials and methods

Measurement setup

Two male subjects (33 and 37 years of age) were imaged at eight UHF sites, all operating a 7 T whole-body MRI system from the same vendor (Siemens Healthcare GmbH, Germany). Data were acquired at the following 7 T sites: 1: Berlin, Germany; 2: Bonn, Germany; 3: Essen, Germany; 4: Heidelberg, Germany; 5: Leipzig, Germany; 6: Maastricht, Netherlands; 7: Magdeburg, Germany; and 8: Vienna, Austria. The sites, all located in Germany and neighboring countries, cooperate within the framework of German Ultrahigh Field Imaging (GUFI).

These systems have differences in basic imaging components that might influence image quality (Table 1). Two sites (2, 6) have an actively shielded magnet installed, which has a smaller warm-bore size (83 vs. 90 cm) and is shorter (2.49 vs. 3.37 m). There are also two different gradient coil versions installed at the different sites: SC72D with 70 mT/m and AS95 with 38 mT/m. The high-performance version (SC72D) provides reduced gradient linearity and is installed at five sites (2, 5–8). At six of the eight sites, a commercial RF head coil (Nova Medical, Inc., Wilmington, MA, USA) with one transmit (TX) and 32 receive (RX) channels is available. A similar 24 RX channel coil from the same manufacturer is available at the other two sites. All systems had the same software version installed (VB17A, 20120320UHFF14).

Table 1 Comparison of 7 T sites

Type of configuration	Magnet type	Gradient coil type	RF coil type	Site	Location
1	Passively shielded	38 mT/m	24 ch	1	Berlin
				4	Heidelberg
2	Passively shielded	38 mT/m	32 ch	3	Essen
3	Passively shielded	70 mT/m	32 ch	5	Leipzig
				7	Magdeburg
				8	Vienna
4	Actively shielded	70 mT/m	32 ch	2	Bonn
				6	Maastricht

The UHF MR systems were from same vendor, but had different hardware components. Four different configurations were identified

To facilitate data analysis, the measurement setup was kept as similar as possible between the sites, and the subjects were positioned as standardized as possible with the help of locally available cushions and pillows. In addition, "auto-align" localizer scans were applied to orient the slice position and angle fully automatically based on anatomical landmarks [13]. This method has been shown to work reliably also at 7 T and lead to higher slice reposition accuracy than manual positioning [14].

The imaging protocol consisted of a vendor-provided spin-echo-based B1 mapping sequence (TR 1200 ms, TE 14 ms, 5 × FA 45°–135°, #SL 11, TA 0:27, 8 × 8 × 5 mm^3) for transmitter calibration, verified by a 3D DREAM [15–17] B1 mapping sequence (TR 5000 ms, TE 0.8/1.5 ms, STE first timing, #SL 36, TA 0:05, 5 × 5 × 5 mm^3). A second order B0 shimming routine of the vendor was applied with the system integrated routine in two iterations. The measurement volume was adjusted manually to include the whole brain. Subsequently, the following imaging sequences were performed: MP2RAGE in sagittal orientation (TR 6000 ms, TI 800/2700 ms, TE 3.0 ms, 3D, TA 9:38 min, 0.75 × 0.75 × 0.75 mm^3), TSE in AC-PC orientation (TR 9000 ms, TE 16/130 ms, #SL 35, SL gap 1 mm, RF pulse length exc./ref.: 3/6 ms, TA 7:05 min, 0.3 × 0.3 × 2.0 mm^3), modified time-of-flight angiography (TOF) [18] (TR 21 ms, TE 4.3 ms, FA 20°, 3D, #SL 112, PAT 4, AC-PC, TA 6:41, 0.2 × 0.2 × 0.4 mm^3), and SWI (TR 29 ms, TE 15 ms, FA 15°, 3D, #SL 112, PAT 3, AC-PC, TA 9:05 min, 0.3 × 0.3 × 1.0 mm^3). An EPI sequence with sinusoidal readout [19] (TR 2350 ms, TE 21 ms, ES 1.03 ms, #SL 46, PAT 3, AC-PC, TA 4:22 min, 1.3 × 1.3 × 1.5 mm^3) was used to acquire T2*-weighted time series data during 4 min of scan time without task. All sequences except TOF and EPI had full brain coverage. For TOF, the imaging slices were centered at the height of the thalamus. The upper border of the EPI slab was set at the level of the most cranial borderline between frontal cortex and subdural space.

Different sequence parameters were chosen at the 24ch coil sites (Sites 1 and 4) and at Site 6 for TSE measurements. The repetition time was increased to 10,000 ms and the number of slices was reduced to 30 (26 at Site 1). At Site 6 an unknown power problem with the RF power amplifier during TSE forced the use of the same reduced duty cycle. For TOF the TR was also slightly increased from 21 to 23 ms at the 24ch coil sites. Due to sequence installation failures at Sites 4 and 6, a multi-shot reference scan was used for phase correction rather than the FLASH reference scan that was conducted otherwise. The FLASH reference scan is less sensitive to subject movements and improves temporal SNR (tSNR) [20]. During a second scan at Site 4, reinstallation of sequence sources allowed both options for the rescans.

Table 2 Chronology of the measurements for the traveling heads study at the different sites

Site	Location	Scans	Date of measurement
1	Berlin	1	(7) 2015/07/20
2	Bonn	2	(2) 2015/01/06, (10) 2015/10/12
3	Essen	3	(1) 2014/10/28, (3) 2015/01/13, (12) 2015/11/03
4	Heidelberg	2	(6) 2015/02/20, (11) 2015/10/28
5	Leipzig	1	(8) 2015/07/21
6	Maastricht	1	(4) 2015/01/19
7	Magdeburg	1	(5) 2015/02/03
8	Vienna	1	(9) 2015/07/30

The order of each scan is indicated by the number in parentheses. The first scan and the latest rescan were acquired at Site 3

The entire protocol was repeated for both subjects on different days at three sites [Sites 2, 3(2×), and 4] to assess intra-system variability. Data acquisition for the study was begun and ended at Site 3, with a time span of 12 months between first and last scan (Table 2).

Data analysis

All measurements were acquired within 1 h per subject, with all inline filters and subsequent data corrections deactivated as far as accessible through the user interface. Gradient distortion correction was applied to all image data except TSE. Registration and image processing was done with FSL [21, 22] (FMRIB Software Library v5.0, The University of Oxford). Brain extraction was performed based on the MP2RAGE de-noised uniform images [23] and brain segmentation was calculated based on the bias-corrected uniform images [24] (Fig. 1). The resulting VOI masks were applied to MP2RAGE images and T1 maps as well as dual-echo TSE. To measure total brain volume with high accuracy, a multi-stage brain extraction was employed based on the optiBET script [25]. This script was used to achieve a first approximate brain extraction. After bias correction with the FSL_anat script, a second run of optiBET with optimized settings was applied, and the extracted brain was registered to the MNI template. FAST [26] tissue type classification with initialization of a priori MNI tissue maps was used. Typical subcortical structures like hippocampus or thalamus were segmented with the run_first_all script [27]. An inferior brain mask was calculated as the sum of brain stem and cerebellum mask to analyze cerebrum and inferior brain separately. All segmented masks were also used for TSE contrast evaluation and were, therefore, transferred to TSE image orientation and resolution with FLIRT [28]. For qualitative analysis a second registration procedure was applied to the MP2RAGE and TSE images. For

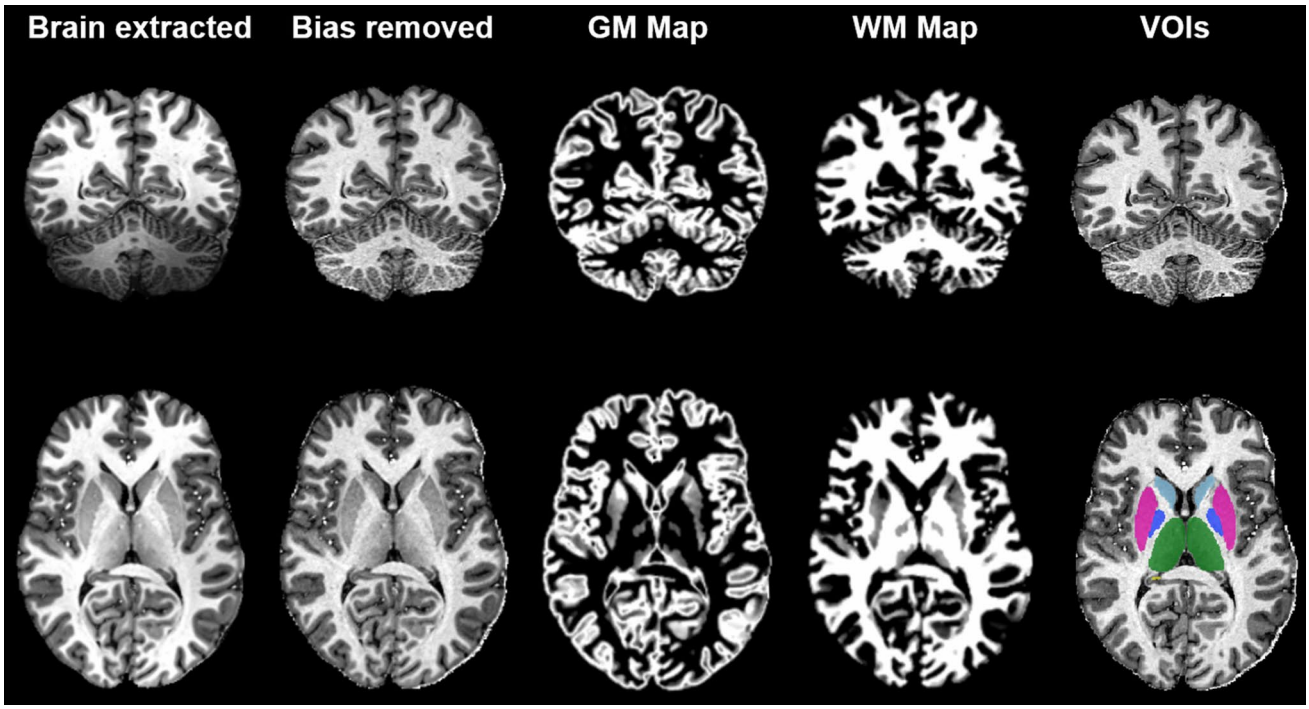

Fig. 1 Post-processing of MP2RAGE images. FSL was used for quantitative image analysis. Brain extraction and tissue type classification were done based on the de-noised uniform images. Subcortical structures were segmented in bias-removed images

this purpose, a template for both subjects was created from all three MP2RAGE scans at Site 3. This template was used to linearly co-register images from the other sites with six degrees of freedom (DOF). TSE were also co-registered using transformation matrices gained from previous calculations. Images from TSE were analyzed for each RF coil in two separate subgroups, as sequence parameters had to be changed for the 24ch coil. The TSE data from Site 6 were excluded from group analysis as unknown power problems and adaption of sequence parameters to those of the 24ch sites resulted in different image contrast. The Michelson contrast definition as the quotient of difference and sum of two different tissue signal intensities was used for all contrast measures between tissues. Mean values, standard deviation between sites, and coefficient of variance (COV) were calculated.

Angiographic image data were co-registered to a single rescan at Site 3 and vessel-to-background contrast was measured for various equally distributed vessels and subcortical regions. For TOF analysis, images were brain-extracted and bias-corrected with FSL. Six volumes of interest were defined by thresholding all vessels in a 30 mm diameter spherical volume (MRIcron, v.6.6, Chris Rorden). Adjacent background tissues were selected manually. The seed points of VOIs were chosen at the most prominent vessels in volumes representing the frontal, left and right frontal, left and right dorsolateral, and central part of the brain (Fig. 2). TOF images of the other sites were co-registered to the latest rescan of Site 3 in two steps. After in-plane subsampling (2×), a 7-DOF registration was applied. For each vessel, the co-registered images were registered a second time using local weighting of the cost function with dilated vessel masks (12 DOF). Maximum intensity projections (MIP) were calculated (ImageJ, v. 1.50e, National Institutes of Health, USA) based on globally registered images for qualitative analysis. To assure that only overlapping brain regions are shown in MIPs, binary brain masks were created, transferred to reference image space, combined using multiplication (logical *and*) and applied. The vessel-to-background contrast was calculated and compared quantitatively. Statistical significance between sites was calculated with Sigmaplot (Sigmaplot 11, Systat Software Inc.). Friedman repeated measures analysis of variance on ranks, Mann–Whitney rank sum test, and Wilcoxon signed rank rest for rescans were used.

The SWI image data were also post-processed with FSL. The latest rescan at Site 3 was defined as the reference dataset, where five equally distributed vessels and surrounding tissue were manually segmented in each subject's brain. The most prominent vessels with a minimum diameter of 15 mm were chosen, representing the frontal, left, right, and central part of the brain (Fig. 2). Additionally, six subcortical volumes and the adjacent background tissues were selected for analysis. Four of them (left/right

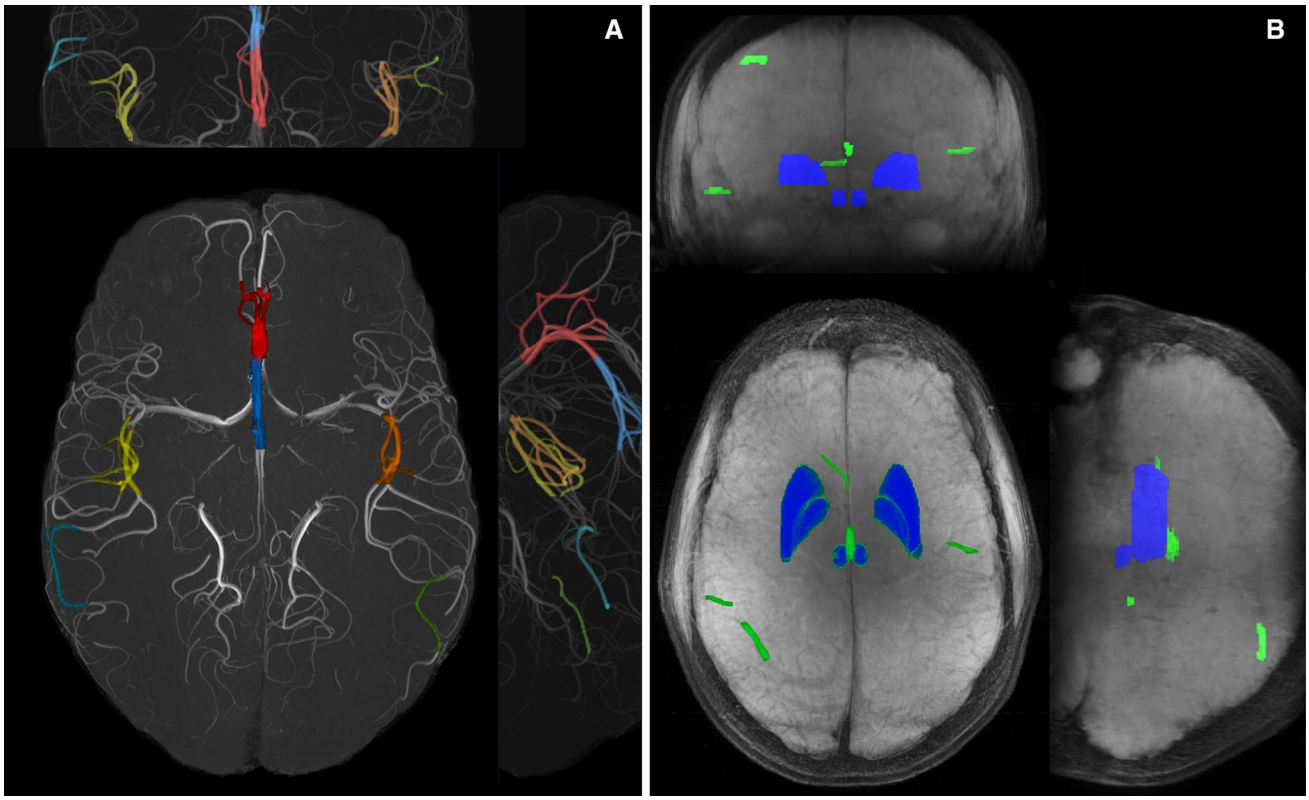

Fig. 2 Selection of vessels and subcortical volumes for angiographic analysis. In (**a**) the *colored overlay* in MIP shows vessel selection for the TOF sequence. In (**b**) the position of vessels and subcortical regions is shown in SWI projections. For TOF, two sections of the pericallosal artery (*red* and *blue*), left and right deep branches of the middle cerebral artery (*yellow* and *orange*), and left and right cortical branches of the middle cerebral artery (*turquoise* and *green*) with surrounding vessels (30 mm) were chosen for analysis. For SWI, subcortical VOIs (*blue*) of left and right putamen, pallidus and red nucleus as well as the five veins with the largest diameter (*marked green*, e.g., internal cerebral veins or parietal superior cerebral vein) in different brain regions were chosen for contrast comparisons. For both subjects the same VOIs were selected

putamen and globus pallidus) were derived from registration of the SWI images to the TSE (3 DOF, auto-align angle for scanning used) and MP2RAGE scans. Left and right red nuclei were manually segmented. From the vessel segmentation, a weighting mask was calculated for each vessel and used for optimization of the cost function of the individual FLIRT registration. Analogous to TOF analysis, a 12-DOF registration was applied for each vessel between the sites to minimize registration errors. The segmented vessel masks were transferred to each site's original image space and vessel-to-background contrast was measured. A second global registration for each brain with 7 DOF and no weighting was also calculated for qualitative analysis. For both angiographic analyses, mean vessel contrast ratio and mean contrast difference of all segmented vessels to reference scan vessels were compared site-wise, and the range of contrast-ratio values was compared vessel-wise.

The EPI scans were co-registered with the help of gradient-echo (GRE) images from the B0 field mapping sequence. The GRE images of a rescan at Site 3 were used as reference, and all other sites were registered to it with FLIRT. Brain extraction was performed, and EPI images and B0 field maps were transferred to reference image space for qualitative analysis. To assure that overlapping brain regions were chosen for quantitative analysis, binary brain masking and a combination of masks was applied similar to TOF. Movement correction with MCFLIRT was applied to all datasets and tSNR was calculated. To analyze system-specific signal drift, tSNR was calculated with and without the application of a high-pass filter (cutoff/FWHM: 235 s). As scaling factors, employed during conversion to integer image data, were not optimally adjusted for the EPI data of Site 8, pixels with high signal level (in regions at the brain surface) were partially saturated at the maximum level. To accommodate this, a filter that excluded the 5 % of voxels with highest signal level was additionally applied to all image data. The brain was extracted with BET on the mean image of all time points, and tSNR was calculated in filtered masks.

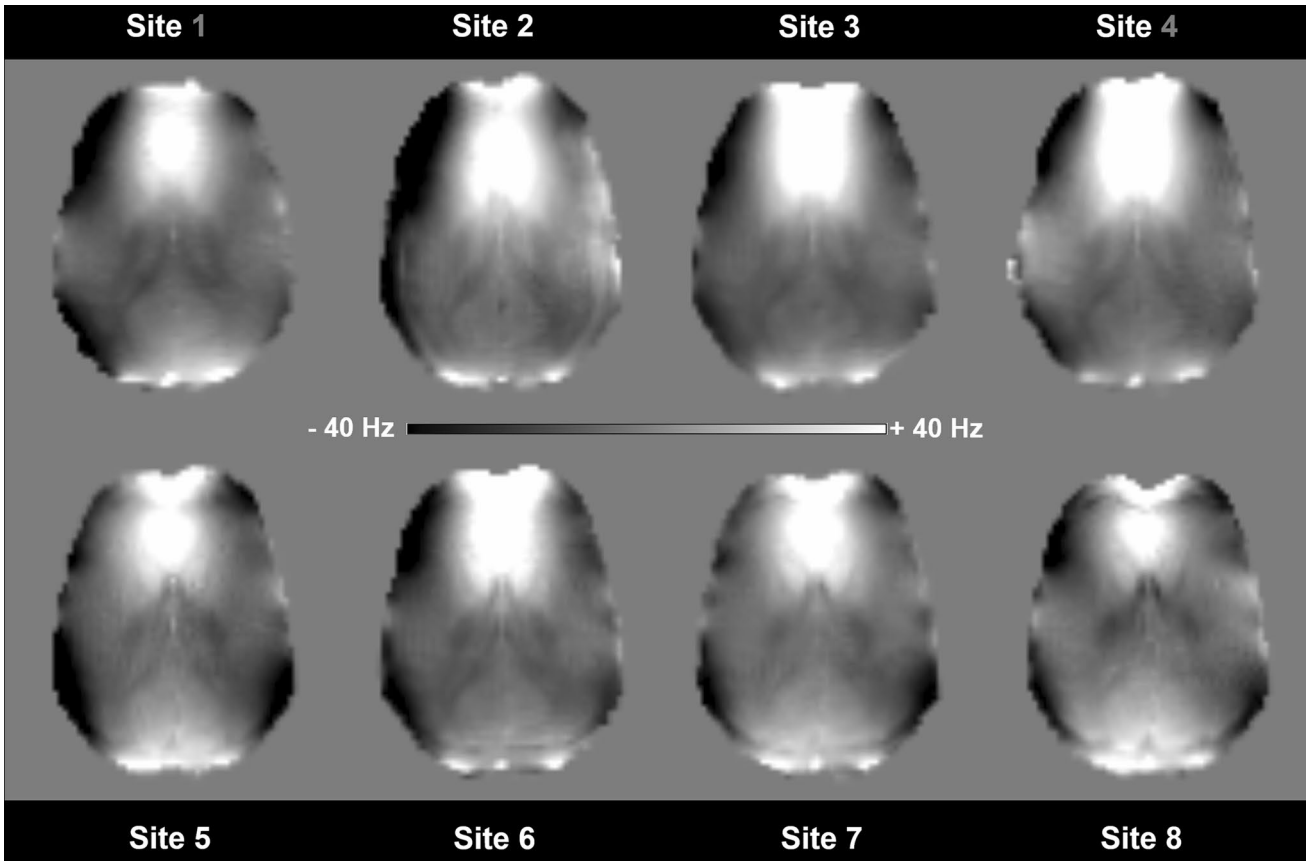

Fig. 3 B0 maps of Subject 1. The same horizontal slice as for the EPI measurement (Fig. 9) is shown. Field homogeneity was slightly different between the measurements

B1 field maps were derived from the DREAM sequence. The brain was extracted from the GRE images of the sequence and applied to the flip angle map. Mean and standard deviation of flip angles were calculated in this volume. Similar analysis was done for the B0 maps, which were registered as described above. The B0 field maps have been calculated with FSL to obtain off resonance in Hertz. Standard deviation and quadratic mean have been analyzed.

Figures 1, 2, 3, 4, 5, 6, 7, 8 , 9 show image data of Subject 1. Tables 1, 2, 3, 4, 5, 6 contain detailed data for both subjects 1 and 2.

Results

The B0 field maps are shown in Fig. 3. For both subjects the lowest absolute field deviation and standard deviation of field map were achieved at Site 7 (Table 3). Repeated measurements at Sites 2, 3 and 4 revealed that absolute field deviation and standard deviation changed by up to 3 Hz between rescans. The B1 maps show differences in the efficiency of the two RF coil types (Fig. 4; Table 3). The 24ch coils reached a mean flip angle of 26°, whereas the 32ch coils achieved 33° with the same transmit power. Differences of up to 4° were found between the sites with identical RF coil types, and rescans at the same site were within 1° difference. The 24ch coil at Site 4 had been replaced between the two scans, but the mean flip angle of the new RF coil did not differ significantly from the one replaced. The 24ch coil that was replaced had a higher relative standard deviation of flip angles (0.33) compared to all other RF coils (0.19–0.26). The flip angle maps of both subjects had similar global values and congruent findings. The calculation of transmit power led to a 14 % higher transmitter reference voltage for the 24ch coil systems compared to the 32ch sites (Table 3).

MP2RAGE images showed very high agreement in contrast and measured T1 values in all regions except the cerebellum and brain stem (Fig. 5; Table 4). Subjects 1 and 2 had a mean brain size of 1494 and 1423 cm^3, respectively. Maximum variation of calculated brain size between the sites was 5 % for Subject 1 and 4 % for Subject 2. Rescans at three sites showed higher intra-site than inter-site reproducibility (max. 0.6 % difference). For smaller subcortical

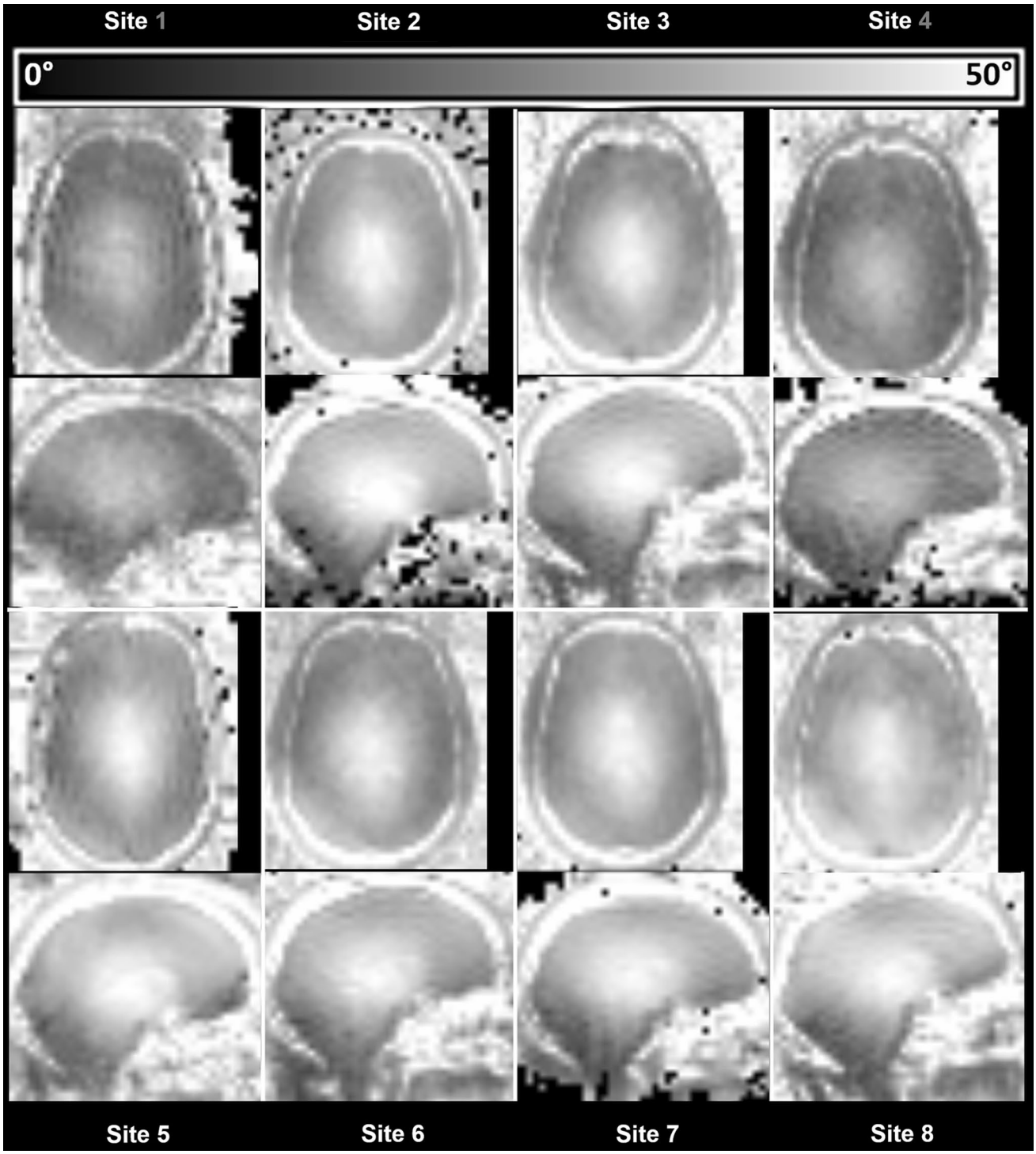

Fig. 4 Flip angle maps of Subject 1. *Axial and sagittal views* are shown for better depiction of differences in inferior brain regions. The 24ch RF coils achieve lower flip angles at the same applied power (Sites 1 and 4)

volumes, intra-site reproducibility was also higher than inter-site deviations (e.g., hippocampus intra-site vs. inter-site COV: 1.3 vs. 3.5 %). Signal levels at inferior brain regions like the cerebellum or brain stem dropped off very fast, and thus tissue segmentation or T1 measurements were more likely to fail in this region. This was observed for different scans of Subject 2. The volumes of gray matter (GM) and white matter (WM) scaled with the total brain volume, but inter-site differences could be reduced to 3 % for Subject 2, when the inferior brain regions were excluded from

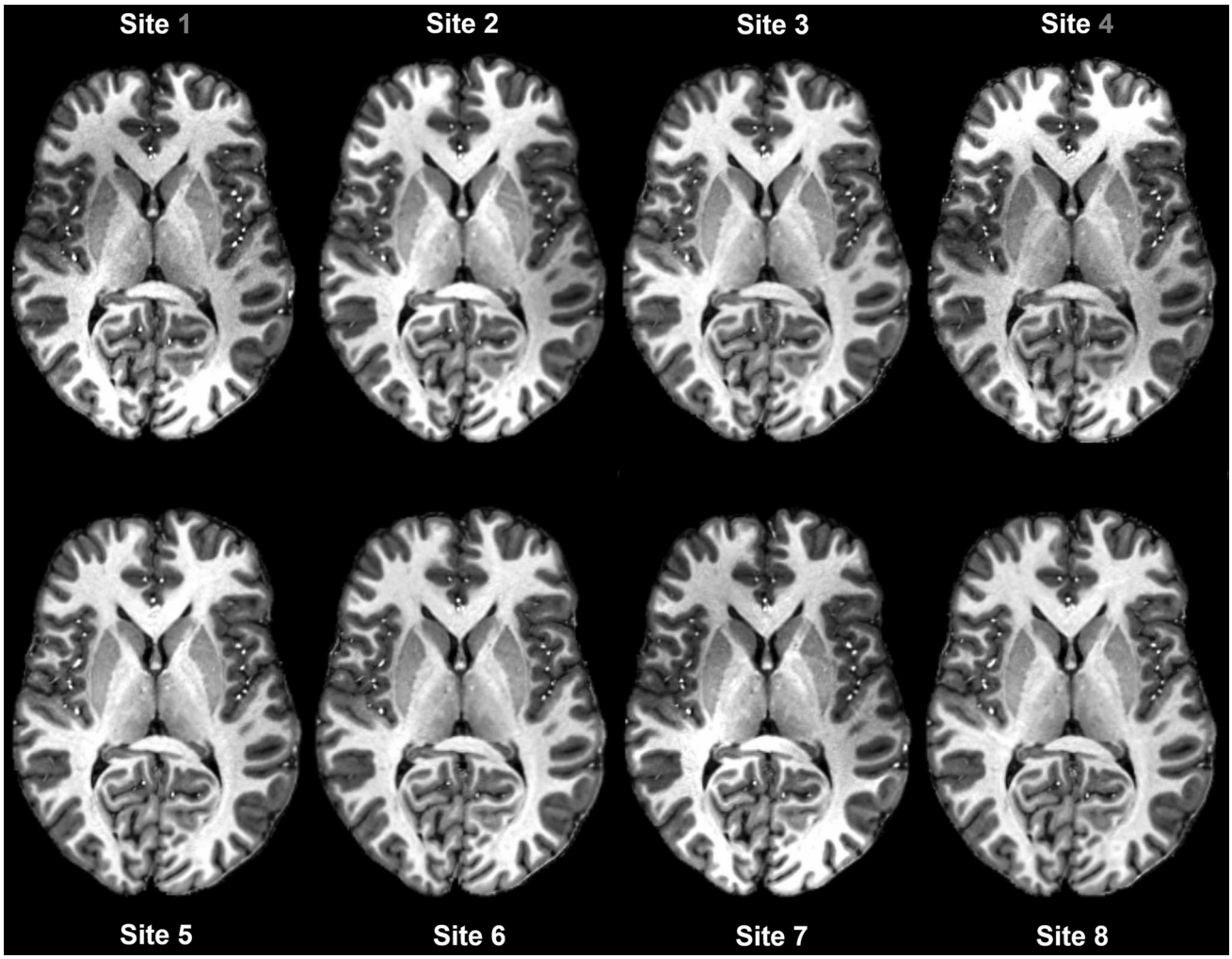

Fig. 5 MP2RAGE uniform image. Horizontal slice through the brain of Subject 1 measured at different 7 T sites. 24ch coil sites (1 and 4) are indicated with a dark grey numeral. Data were co-registered and brain extracted. MP2RAGE images show high agreement in image contrast at different sites

the analysis. The contrast ratio between GM and WM was very similar between the subjects (mean 0.46 vs. 0.44) and the variation between the sites was minimal (±0.02). Very high reproducibility was found for T1 maps generated from MP2RAGE images (Table 4). Inter-site variation was up to 3 % for all segmented volumes, except for inferior regions like the brainstem and the cerebellum, where T1 calculation failed at some sites due to low signal. With less than 4 %, inter-subject variation was similar. Differences in intra-site reproducibility between the first and the last scan at Site 3 were not found; these scans were the first and last measurements of the entire study and thus had the longest time span of ~12 months between repeated measurements.

The TSE images (Fig. 6) revealed contrast differences between the two different RF coils used. The 24ch coil demanded more transmit power (after flip angle calibration), and thus the SAR prognosis for the TSE exceeded the regulatory limits, because the scanner software used identical SAR limits for both RF coils; consequently, the sequence parameters had be changed (TR, #slices). The contrast ratio of GM to WM was much higher in T2-weighted images than in PD weighting; contrast deviations between the sites did not change for either echo. The maximum gray to white matter contrast differences between all sites were below 8 %. When excluding inferior regions (cerebellum and brainstem) from analysis and grouping the sites coil-wise, total contrast differences were less than 2 % for Subject 1 and 5 % for Subject 2 (Table 5). However, in central subcortical regions, larger contrast deviations up to 22 % were found between the sites with different RF coils, confirming qualitative image impressions as seen in Fig. 6. The coil-wise comparison of subcortical contrast ratios showed a much better agreement between the sites of

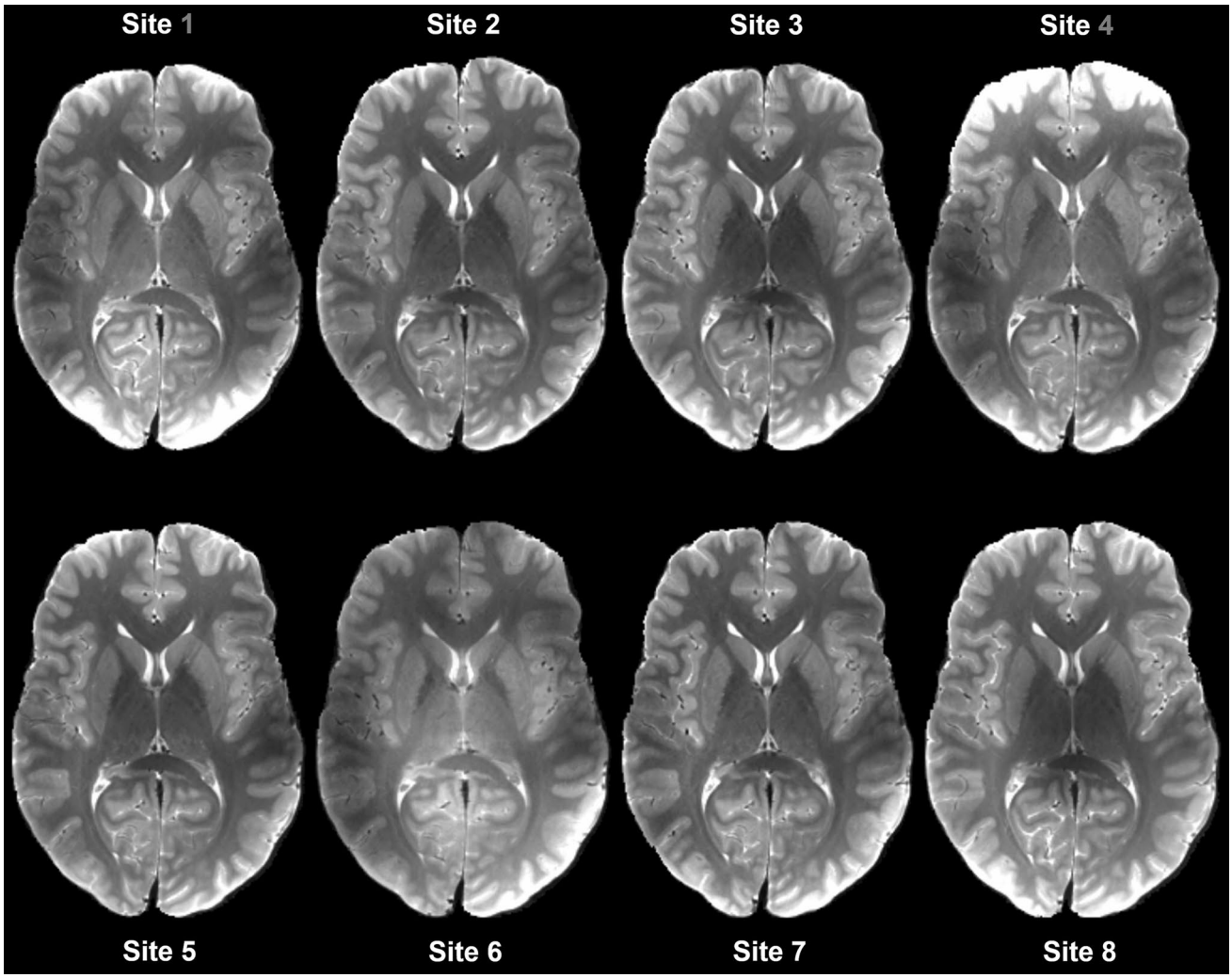

Fig. 6 PD-weighted TSE images from the same horizontal slice as for MP2RAGE of Fig. 5. Sites 1 and 4 (24ch coil) had slightly adapted sequence parameters (TR 10,000 vs. 9000 ms, 30 vs. 34 slices). High agreement was obtained for the sites with identical RF coils except for Site 6, where RF power problems led to a different appearance

less than 10 % difference. For inferior regions like the cerebellum and the brainstem, RF signal drop offs as in MP2RAGE caused high contrast differences between the sites (Table 5).

The TOF angiography (Fig. 7) analysis showed high agreement between all sites and subjects. Mean vessel contrast ratio was very similar between the subjects (0.43 vs 0.41), but higher deviations and lower mean vessel contrasts were found for sites with 24ch RF coils (Table 6). Statistically significant inter-site differences were found with Friedman repeated MANOVA on ranks for Sites 1, 4, and 8. A Mann–Whitney rank sum test ($p < 0.001$) revealed statistical differences between the vessel contrasts of different RF coils. Rescans at three sites showed high reproducibility, and no statistically significant intra-site contrast differences were found. Mean intra-site vessel contrast deviation was lower than mean inter-site vessel contrast deviation (2.3 vs. 3 %). When using the same type of RF coil, the maximum contrast differences between all individual vessels were 11 % for 32ch RF coils and 9 % for 24ch RF coils.

SWI image data (Fig. 8) of the vessels and the subcortical VOIs were analyzed separately in two subgroups. Variation of mean vessel contrasts and mean deviation of contrasts (Table 6) were comparable to TOF analysis, but did not show differences between the RF coils. Inter-subject variation was higher than inter-site variation. In contrast, only minor inter-site and inter-subject differences in mean contrast ratios were measured for subcortical volumes. For both groups, intra-site vessel contrast deviation was lower than mean inter-site vessel contrast deviation (vessels 3.6 vs. 4.1 %, VOIs 1.0 vs 1.6 %). The maximum difference

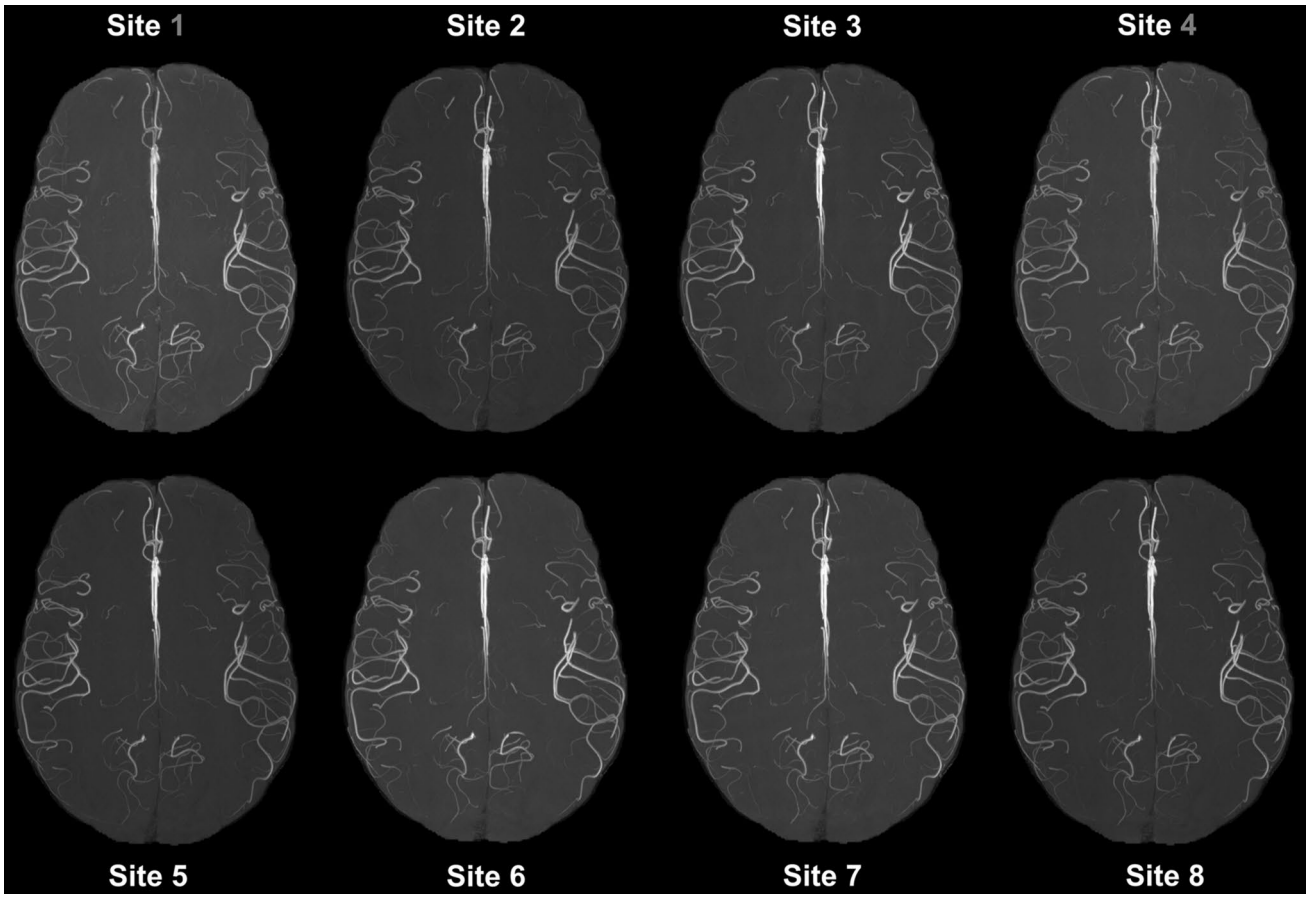

Fig. 7 Maximum intensity projections calculated for each site from TOF angiography of Subject 1. The TOF images were co-registered to the last rescan of Site 3 and masked with the overlapping portion of co-registered data from all sites

in contrast ratios was 14 % for single vessels and 6 % for subcortical VOIs.

EPI images showed typical artifacts at tissue boundaries and air cavities. These artifacts differed in extent over the sites (Fig. 9). These distortion artifacts correspond well with the B0 maps of Fig. 3. The mean tSNR is 15–25 % lower for the sites with 24ch coils compared to those with 32ch coils (Table 3). Site 6 was excluded from the 32ch-coil means, as the tSNR there was similar to that achieved with the 24ch coils because the sequence parameters had to be adapted at this site. Masking the 5 % of voxels with highest signal also reduced the tSNR by about 7 % for Subject 2 and 2 % for Subject 1, but differences between sites were not affected. Subject 1 had a higher agreement of tSNR between the sites: all values were within 11 % difference for the 32ch coil sites. For Subject 2 the span of measurement values was 18 % due to higher tSNR achieved at Site 7. The high-pass filter increased the mean tSNR for the 32ch sites by 6 % but reduced inter-site variability only for Subject 1 by 4 %.

Discussion

The B0 field maps showed slight differences between the sites, but no correspondence to hardware differences like the magnet or the gradient coil type was found. Intra-site differences were on the same level as inter-site differences. Causes other than the actual hardware seem to have a stronger influence on the results of the shimming routines for whole-brain shimming. Possible sources for differences in the field homogeneity are the positioning of the subject in the coil relative to the magnet, but also differences in the chosen adjustment volume. Nevertheless, all B0 maps showed similar field patterns and corresponded well with distortion artifacts found in the EPI images. In contrast, the B1 maps revealed clear differences between RF coils. The transmitter reference amplitude of the 24ch coils was set about 14 % higher to reach a comparable flip angle in a central cubic (50 mm, isotropic) brain region. This was measured with the vendor provided transmitter calibration method. The DREAM validation revealed higher flip

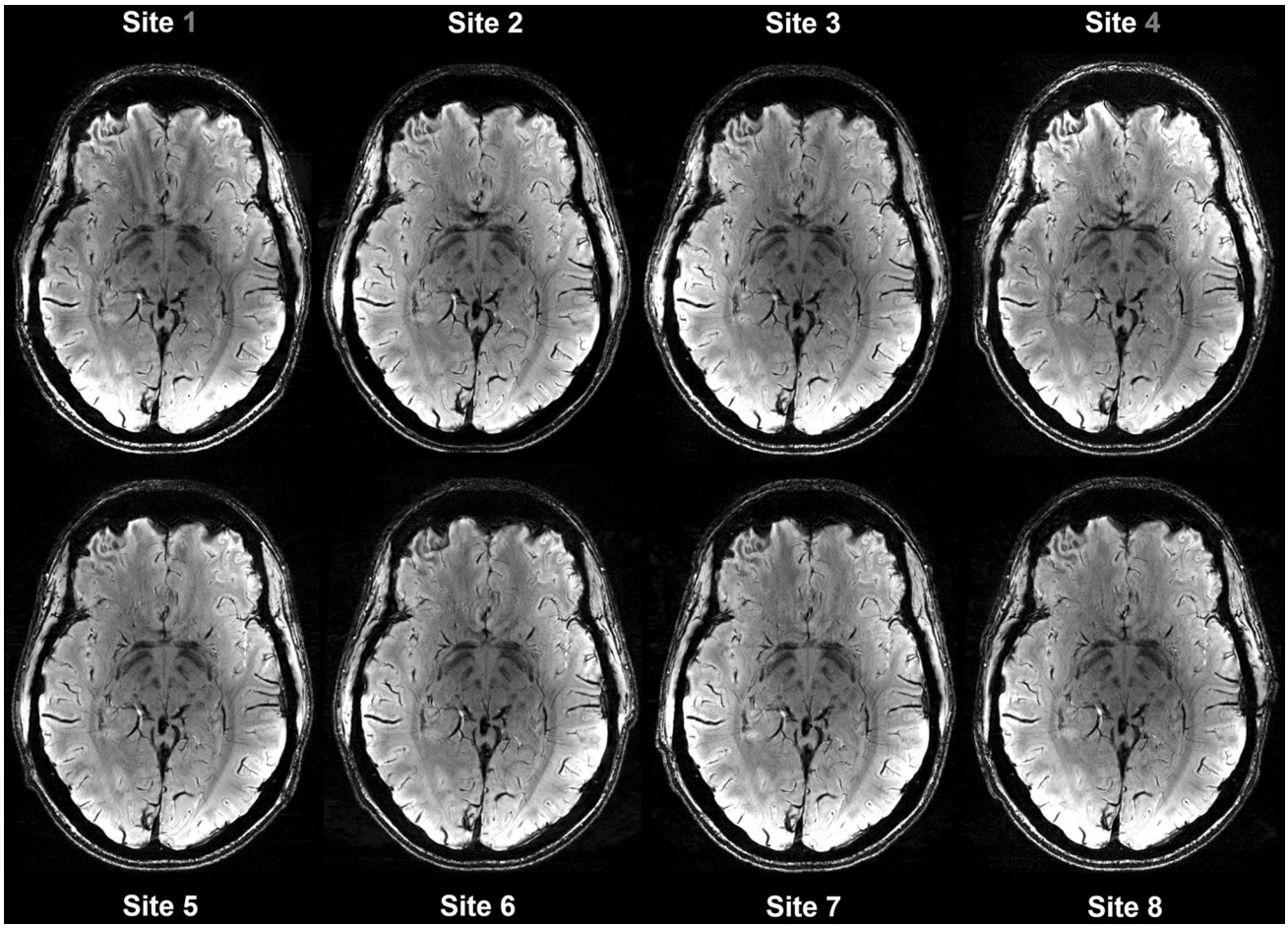

Fig. 8 SWI horizontal slice of Subject 1. Data were registered to the last scan at Site 3. Nine equally distributed vessels and surrounding tissue were manually selected in the reference dataset. Each vessel mask was transferred back to original image space with individually optimized registration parameters

angle differences (26 %) between the two RF coils, while the mean flip angle was calculated for the whole segmented brain. The differences reflect the differently analyzed volumes and indicate that the 32ch coil is more effective in peripheral regions of the brain. Since there is no gold standard for B1 mapping at 7 T, there may be differences due to the used methods as well. At peripheral regions like the inferior brain, inter-site reproducibility of the flip angle maps were reduced. The cerebellum is at the edge of the transmit field of both RF coils, and large differences were observed in the B1 maps and in the actual imaging sequences. Small differences may also result from minor geometric differences in coil shape and resulting head position in the scanner. Differences between the systems were confirmed by rescans at three sites, where the reproducibility difference was small compared to the inter-site difference (1° vs. 4°). Inaccuracies in the power calibration provided by the system vendor or defective hardware may also influence the available RF power and, therefore, limit the maximum achievable flip angle. One system was found where the power calibration was incorrect, leading to reduced possible flip angles and higher SAR prediction than at the other sites. After recalibration of the system by the vendor, the measurement was repeated and B1 mapping results were similar to the other 32ch coil sites.

The MP2RAGE sequence is a fast 3-D gradient-echo sequence with two inversions and is often used as an anatomical T1-weighted scan of the brain to visualize cortical subregions and possibly to align other measurements. This sequence or its derivatives are used at different field strengths in most brain measurement protocols, and a high agreement between the 7 T sites is very important for future multicenter trials. At 7 T, optimized adiabatic inversion pulses (TR-FOCI [29]) are used to overcome limitations in B1 homogeneity. We found that MP2RAGE provided high image quality at all sites and was suitable for automatic analysis with FSL. Volumetric analysis based on MP2RAGE images revealed small inter-site differences

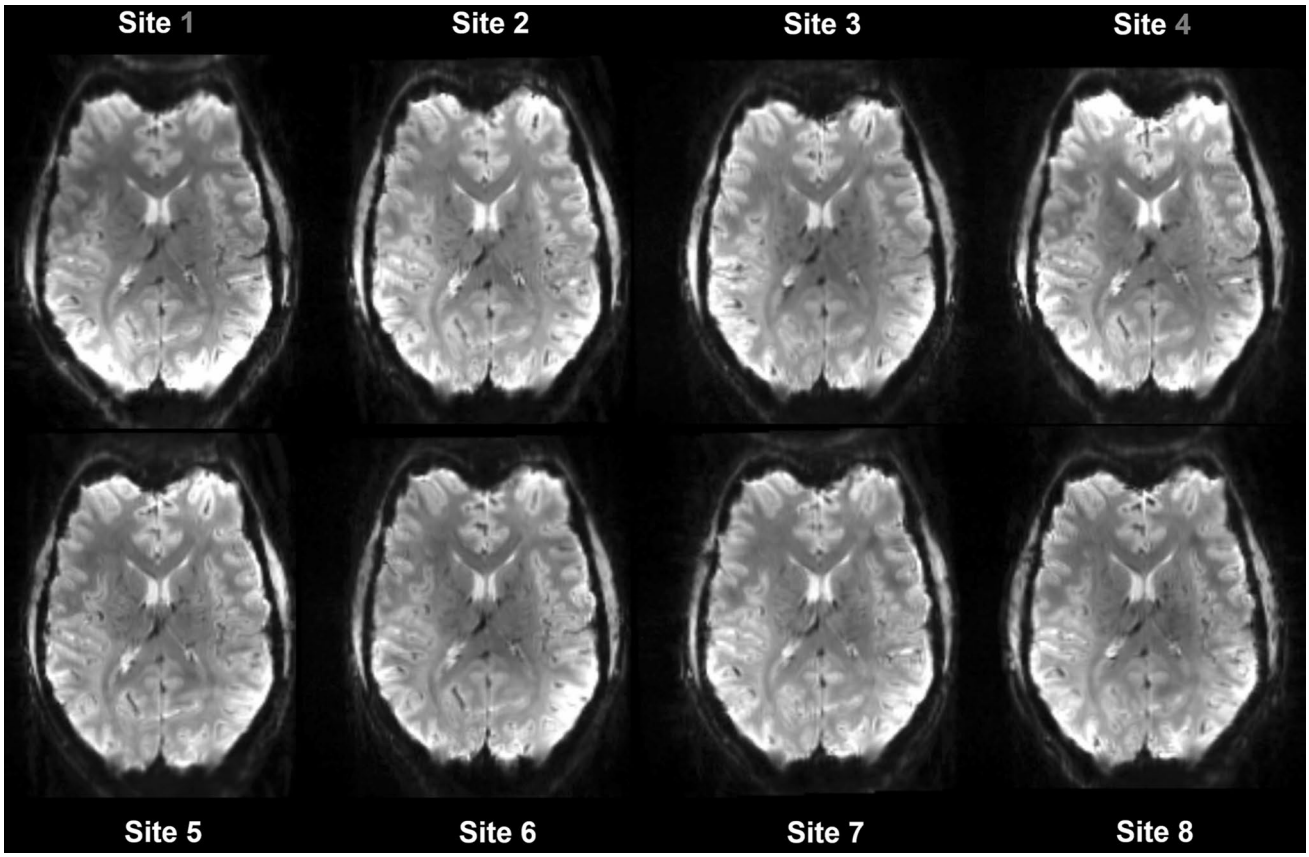

Fig. 9 EPI slice of Subject 1. Local differences due to slightly different artifact levels can be seen. The corresponding slice from the B0 field map shown in Fig. 3 correlates well with the artifacts in the images

Table 3 EPI and fieldmap data for both subjects

		Site 1	Site 2	Site 3	Site 4	Site 5	Site 6	Site 7	Site 8
EPI									
Subject 1	tSNR	41.1	53.3	54.9	39.8	53.9	39.6	49.2	51.4
	tSNR/%	0.75	0.97	1.00	0.72	0.98	0.72	0.89	0.94
	tSNR highpass	45.1	57.3	59.3	41.2	57.9	42.2	54.9	55.4
Subject 2	tSNR	39.9	44.0	43.1	36.3	46.8	39.1	52.8	43.3
	tSNR/%	0.75	0.83	0.82	0.69	0.89	0.74	1.00	0.82
	tSNR highpass	43.0	44.9	44.1	39.2	51.6	40.2	54.9	44.1
B0 mapping									
Subject 1	Stdev. field/Hz	21.9	28.5	23.1	24.5	23.4	22.5	20.1	20.4
Subject 2	Stdev. field/Hz	25.1	25.0	24.5	23.2	20.9	25.1	20.1	22.5
B1 mapping									
Subject 1	Reference voltage	241	228	213	248	213	225	202	213
	Flip angle/°	27.0	32.5	32.4	25.5	33.9	32.5	31.9	35.8
	Stdev. flip angle/°	6.3	7.8	7.1	5.0	8.1	7.8	7.7	9.1
Subject 2	Reference voltage	252	223	227	259	214	234	216	227
	Flip angle/°	27.9	33.0	32.7	25.6	33.6	34.0	31.8	35.8
	Stdev. flip angle/°	7.5	7.9	7.8	5.0	8.4	9.0	7.6	9.1

of 5 %, but rescans at three sites showed almost 10-times higher intra-site reproducibility. The differences showed no tendency to correlate with the hardware of the systems, e.g., either the type of the gradient or RF coil, nor were differences in image quality or the image processing results found or tendencies in B0 or B1 field maps detected that

Table 4 Excerpt of quantitative analysis of MP2RAGE sequence

	Site 1	Site 2	Site 3	Site 4	Site 5	Site 6	Site 7	Site 8	Mean	COV
MP2RAGE										
Volume Subject 1										
Brain volume/cm^3	1468	1506	1465	1530	1471	1509	1500	1507	1494	1.6 %
% Diff. GM Vol.	0.94	0.98	0.96	1.00	0.96	0.99	0.97	0.97	624	1.8 %
% Diff. WM Vol.	0.97	0.97	0.95	1.00	0.96	0.98	0.98	0.99	745	1.5 %
Putamen/cm^3	11.9	11.8	11.9	12.2	11.7	11.3	11.5	11.8	11.8	2.2 %
Hippocampus/cm^3	9.9	9.7	9.7	10.2	9.6	9.2	10.2	9.7	9.8	3.4 %
Cerebellum/cm^3	115	123	132	111	138	158	121	124	128	11.7 %
Volume Subject 2										
Brain volume/cm^3	1390	1438	1409	1445	1394	1435	1438	1434	1423	1.5 %
% Diff. GM Vol.	0.93	0.97	0.95	0.98	0.93	0.97	0.97	0.97	539	2.2 %
% Diff. WM Vol.	0.98	0.97	0.97	0.99	0.98	0.98	0.98	1.00	718	1.0 %
Putamen/cm^3	11.0	10.6	10.8	10.9	11.0	10.5	11.0	11.0	10.8	2.0 %
Hippocampus/cm^3	9.8	9.9	10.0	10.0	9.7	9.1	9.2	10.0	9.7	3.6 %
Cerebellum/cm^3	125	130	144	112	136	120	135	140	130	8.2 %
GM to WM										
Subject 1 (S. 1)	−0.46	−0.47	−0.45	−0.46	−0.44	−0.45	−0.47	−0.44	−0.46	−1.4
Subject 1 (S. 2)	−0.45	−0.47	−0.44	−0.46	−0.42	−0.44	−0.47	−0.43	−0.45	−1.6
T1 values/ms										
GM *(S. 1)*	1912	1905	1914	1918	1902	1915	1920	1898	1925	0.4 %
GM *(S. 2)*	1905	1917	1940	1930	1919	1937	1927	1944	1927	0.7 %
WM *(S. 1)*	1215	1212	1223	1214	1208	1219	1221	1206	1215	0.5 %
WM *(S. 2)*	1247	1251	1258	1255	1249	1255	1264	1255	1254	0.4 %
Putamen *(S. 1)*	1539	1527	1542	1542	1531	1545	1554	1526	1538	0.6 %
Putamen *(S. 2)*	1487	1476	1474	1489	1479	1488	1487	1486	1483	0.4 %
Globus Pall. *(S. 1)*	1203	1182	1201	1196	1184	1203	1203	1184	1194	0.8 %
Globus Pall. *(S. 2)*	1207	1186	1194	1202	1198	1196	1206	1194	1198	0.6 %
Hippocamp. *(S. 1)*	1813	1804	1817	1813	1824	1838	1819	1812	1818	0.5 %
Hippocamp. *(S. 2)*	1765	1777	1783	1785	1771	1781	1783	1793	1780	0.5 %
Cerebellum *(S. 1)*	1267	1691	1686	1608	1650	1729	1542	1693	1608	9.3 %
Cerebellum *(S. 2)*	1005	1656	1680	1520	1360	1710	1459	1555	1493	15.4 %

Data for both Subject 1 and Subject 2 are shown. Coefficient of variation (COV) indicates inter-site deviation. The brain volume was taken as intracranial tissue volume, meaning that the cerebrum, cerebellum and brain stem were included but CSF spaces such as the ventricles were excluded

would indicate systematic differences between the sites. The small discrepancy between inter-site and intra-site reproducibility may be caused by the current calibration of the gradient coils or by other site-specific effects. Nevertheless, the MP2RAGE images showed a very high agreement regarding contrast measures and provided very precise T1 relaxation maps for all reviewed structures of the brain except the inferior parts such as the cerebellum and brain stem, where signal levels dropped consistent with the B1 loss measured there. The 7 T systems we compared were all from the same vendor and shared a lot of common hardware and software, but there were also differences in the hardware components, e.g., the magnet designs or the gradient coils. This leads to lower inter-site than intra-site reproducibility. Of course, a comparison across different vendors of MR systems would have been advantageous to include more differences in gradient coil designs and sequence programming. However, it should be kept in mind that at all currently installed 7 T sites, independent of the MR system vendor (Philips, GE, Siemens), both the magnet and the head RF coil come from the same vendors (Agilent and Nova Medical). This leaves mainly the signal generation and reception as well as possible differences in sequence programming as remaining sources of variation between vendors, which may lead to even lower variability as compared to 3 T. A rough comparison to volumetric measurements at 1.5 and 3 T made by Huppertz et al. [30] can be made. However, they used SPM to calculate and compare the intracranial volume as well as GM, WM, and CSF maps for one subject who was measured three times

Table 5 TSE contrast measures

	Weighting	Contrasts	GM to WM	Putamen	Hippocampus	Brainstem	Cerebellum
TSE 32ch coils							
Subject 1	PD	Mean	0.18	0.23	0.26	0.17	0.10
		Span ±	0.02	0.04	0.05	0.05	0.16
	T2	Mean	0.27	0.07	−0.07	0.24	0.26
		Span ±	0.01	0.02	0.02	0.02	0.02
Subject 2	PD	Mean	0.15	0.19	0.22	0.10	−0.04
		Span ±	0.05	0.03	0.06	0.05	0.11
	T2	Mean	0.25	0.04	−0.10	0.18	0.18
		Span ±	0.03	0.01	0.03	0.03	0.03
TSE 24ch coil							
Subject 1	PD	Site 2	0.17	0.15	0.12	0.13	−0.07
		Site 4	0.17	0.16	0.14	0.09	0.00
	T2	Site 2	0.27	0.06	−0.09	0.17	0.20
		Site 4	0.25	0.07	−0.06	0.20	0.19
Subject 2	PD	Site 2	0.13	0.11	0.06	0.00	−0.36
		Site 4	0.14	0.13	0.13	0.09	−0.05
	T2	Site 2	0.23	0.03	−0.13	0.09	0.08
		Site 4	0.24	0.04	−0.12	0.13	0.15

The contrast between different tissues was compared coil-wise for the TSE sequence. Image contrast of subcortical structures was measured relative to the globus pallidus

Table 6 Excerpt of angiography analysis

	Site 1	Site 2	Site 3	Site 4	Site 5	Site 6	Site 7	Site 8	Reference
TOF									
Subject 1									
Vessel contrast	0.41	0.48	0.44	0.42	0.47	0.47	0.46	0.49	0.42
Mean deviation	0.04	0.04	0.03	0.05	0.03	0.02	0.02	0.05	
Subject 2									
Vessel contrast	0.36	0.41	0.44	0.35	0.43	0.42	0.42	0.44	0.44
Mean deviation	0.08	0.03	0.01	0.09	0.03	0.02	0.02	0.01	
SWI									
Subject 1									
Vessel contrast	−0.71	−0.70	−0.74	−0.69	−0.71	−0.71	−0.70	−0.72	−0.72
Mean deviation	0.04	0.02	0.03	0.04	0.02	0.05	0.03	0.05	
Subcortical contrast	−0.24	−0.25	−0.25	−0.26	−0.26	−0.26	−0.26	−0.26	−0.26
Mean deviation	0.03	0.02	0.01	0.01	0.01	0.01	0.02	0.01	
Subject 2									
Vessel contrast	−0.78	−0.76	−0.78	−0.78	−0.76	−0.76	−0.77	−0.76	−0.82
Mean deviation	0.04	0.06	0.04	0.04	0.05	0.06	0.04	0.06	
Subcortical contrast	−0.24	−0.23	−0.23	−0.24	−0.23	−0.24	−0.24	−0.23	−0.24
Mean deviation	0.02	0.01	0.01	0.01	0.02	0.01	0.01	0.01	

Vessel contrast is the mean between all segmented vessels per site. The mean deviation is the absolute mean of each vessels difference to the reference scan

on six different 1.5 and 3 T devices from two vendors. They reported mean intra-site coefficients of variation (COV) for brain, WM, GM, and CSF volumes of 0.5, 0.7, 0.7, and 4.4 % and respective inter-site COVs of 3.8, 3.7, 4.1, and 8.7 %. Our inter-site results show higher inter-site reproducibility, which may reflect that the systems used were all from the same vendor. The intra-site reproducibility, which can be extracted for Site 3 from two subjects with three repetitions (COV 0.2, 0.9, 1.3, and 1.9 %), shows similar results as described for the other field strengths. Differences may also result from the different segmentation methods used [7, 31, 32]. Other groups [33] also

reported high intra-site reproducibility for 1.5 and 3 T, but differences across platforms and across field strengths were found. In contrast to lower field strengths, the performance of the setup employed at 7 T in our study cannot be used to reliably quantify the infratentorial brain region, as signal level is too low there. Further optimization of RF coils is needed to overcome these limitations to exploit the higher signal level achievable with 7 T. However, the supratentorial brain reproducibility is very high, which is a promising finding for the reliability of the compared systems.

The TSE sequences are the classical workhorses of MRI at most field strengths and a widely accepted robust imaging method. At UHF, different adaptations were made to overcome SAR limitations that arise at higher field strength due to the quadratic dependency of RF power on Larmor frequency. The sequence we employed utilizes hyperechos [34], allows regulation of pulse lengths, and uses the VERSE [35] algorithm to reduce peak pulse power and thereby the SAR. The SAR limit is always critical for TSE at 7 T and forced us to change the sequence parameter for the 24ch coils, as the scanner software did not account for the lower transmit efficiency of this older coil version compared to the 32ch coil, which was used to set up the imaging protocol. The different sequence parameters led to slightly different contrasts between the sites with different RF coils, especially in central subcortical VOIs. It cannot be assumed, however, that contrast differences would not have occurred if identical sequence parameters had been used because the B1 maps also differed between the RF coils. Site 6 was excluded from analysis, as unknown power restrictions did not allow similar sequence parameters as for the other 32ch coils. Results of the coil-wise comparisons showed strong inter-site correspondence and high reproducibility.

TOF measurements are also challenging at 7 T as the SAR limits are critical due to the applied saturation pulses; the measurements benefit, however, as contrast-to-noise ratio is much higher due to longer T1 relaxation times. The sequence used allowed the regulation of saturation flip angle independent of excitation flip angle and also had the VERSE pulse modification implemented to reduce SAR. At the 24ch coil sites, TR was increased slightly (23 vs. 21 ms) to meet SAR restrictions. Differences between the sites were found, as vessel contrast was slightly reduced for most vessels at the 24ch coil sites. For the two chosen dorsolateral branches of the middle cerebral artery, differences between the RF coils were similar to inter-site variations. This may be due to the different receive (or transmit) sensitivities of the RF coils, but may also originate from physiological parameters like heart rate or blood pressure. Other reasons like subject positioning can also not be excluded. The TOF images and the calculated MIPs show very high agreement, and the similarity in measured vessel contrasts indicates that vessel resolution is comparable between sites.

SWI benefits from higher susceptibility sensitivity at 7 T. Therefore, very small veins can be depicted with SWI. To reach whole-brain coverage in reasonable measurement time (~10 min), a slice resolution of 1 mm was chosen, and the resulting voxel size was bigger than for TOF [$(0.3 \times 0.3 \times 1)$ vs. $(0.2 \times 0.2 \times 0.4)$ mm^3], where a smaller central slab was imaged, and more highly anisotropic. This led to higher interpolation errors and partial volume effects when relatively small vessels compared to bigger subcortical structures were chosen for quantitative comparison. Nevertheless, the larger veins we chose for analysis had only minimally larger deviations between sites than the arteries compared with TOF. For all subcortical structures, the differences between the sites were minor and much lower than for the TOF measurements. The differences in TOF may be caused by the different contrast mechanisms of the sequences, as indicated by RF coil differences found with TOF, but also physiological reasons like blood flow variations may play an important role.

EPI is very fast and therefore very useful in applications such as functional imaging, but prone to imaging artifacts due to B0 inhomogenities or susceptibility effects. The sequence we used had a modified reference scan for phase correction to account for the higher sensitivity of 7 T to susceptibility and also a sinusoidal readout to reduce gradient coil resonances and helium boil-off. At Site 6 and for the first scan at Site 4, this type of reference scan was not available due to sequence installation problems, and tSNR values were slightly lower than at comparable sites. The distortion artifacts seen in the EPI images correlated well with measured B0 variations. The 32ch coil sites had a higher mean tSNR than the 24ch coil sites. This also corresponds well with other findings at 3 and 7 T [36–38]. It has been shown that tSNR benefits most from higher field strength or highly parallel arrays when thermal noise is dominant, e.g., for small voxel volumes and for higher acceleration factors, as in the applied sequence. Inter-site variation of tSNR was smaller for Subject 1 than for Subject 2, and this difference was even increased by the correction for scanner drift. This may indicate that corrections were disturbed by subject movement, physiological effects, or other side effects that could not be detected.

Conclusion

UHF MR systems are very sensitive measurement devices, but high sensitivity also applies to noise and susceptibility to hardware faults. Even for systems provided from the same vendor, there can be remarkable differences between basic imaging components of the individual MR systems and sites that potentially might influence image quality. Effects of these hardware differences were revealed in this study, where

it could be shown that the RF coils had the greatest effect on inter-site reproducibility; the effect of the gradient coils and magnet type was more limited. Nevertheless, our results show that the 7 T systems used can deliver high multi-center reproducibility for the supratentorial brain with variability that is similar to that reported in the literature for 3 T. This is a promising finding for quantitative imaging, and a first step toward future large scale multi-site studies at 7 T.

Compliance with ethical standards

Funding This work was support by a Grant of the German Research Foundation (DFG)/project German Ultrahigh Field Imaging/Grant n. LA 1325/5-1. UHF adapted imaging sequences were provided by Siemens Healthcare.

Conflict of interest The authors declare that they have no conflict of interest.

Ethical standards All procedures performed in studies involving human participants were in accordance with the ethical standards of the institutional and/or national research committee and with the 1964 Helsinki declaration and its later amendments or comparable ethical standards.

Informed consent Informed consent was obtained from all individual participants included in the study.

References

1. Kraff O, Fischer A, Nagel AM, Monninghoff C, Ladd ME (2015) MRI at 7 Tesla and above: demonstrated and potential capabilities. J Magn Reson Imaging 41(1):13–33
2. Bernstein MA, Huston J 3rd, Ward HA (2006) Imaging artifacts at 3.0T. J Magn Reson Imaging 24(4):735–746
3. Ugurbil K (2014) Magnetic resonance imaging at ultrahigh fields. IEEE Trans Biomed Eng 61(5):1364–1379
4. Balchandani P, Naidich TP (2015) Ultra-high-field MR neuroimaging. AJNR Am J Neuroradiol 36(7):1204–1215
5. Opderbeck T (2015) New 7 Tesla MRI research system ready for future clinical use. Siemens Healthcare GmbH. http://www.siemens.com/press/PR2015060231HCEN. Accessed 08 Dec 2015
6. Jovicich J, Marizzoni M, Sala-Llonch R, Bosch B, Bartres-Faz D, Arnold J, Benninghoff J, Wiltfang J, Roccatagliata L, Nobili F, Hensch T, Trankner A, Schonknecht P, Leroy M, Lopes R, Bordet R, Chanoine V, Ranjeva JP, Didic M, Gros-Dagnac H, Payoux P, Zoccatelli G, Alessandrini F, Beltramello A, Bargallo N, Blin O, Frisoni GB (2013) Brain morphometry reproducibility in multi-center 3 T MRI studies: a comparison of cross-sectional and longitudinal segmentations. Neuroimage 83:472–484
7. Mulder ER, de Jong RA, Knol DL, van Schijndel RA, Cover KS, Visser PJ, Barkhof F, Vrenken H (2014) Hippocampal volume change measurement: quantitative assessment of the reproducibility of expert manual outlining and the automated methods FreeSurfer and FIRST. Neuroimage 92:169–181
8. Teipel SJ, Meindl T, Grinberg L, Heinsen H, Hampel H (2008) Novel MRI techniques in the assessment of dementia. Eur J Nucl Med Mol Imaging 35(Suppl 1):S58–S69
9. Mueller SG, Weiner MW, Thal LJ, Petersen RC, Jack C, Jagust W, Trojanowski JQ, Toga AW, Beckett L (2005) The Alzheimer's disease neuroimaging initiative. Neuroimaging Clin N Am 15(4):869–877 **(xi-xii)**
10. Seiger R, Hahn A, Hummer A, Kranz GS, Ganger S, Kublbock M, Kraus C, Sladky R, Kasper S, Windischberger C, Lanzenberger R (2015) Voxel-based morphometry at ultra-high fields. A comparison of 7 T and 3 T MRI data. Neuroimage 113:207–216
11. Lusebrink F, Wollrab A, Speck O (2013) Cortical thickness determination of the human brain using high resolution 3 T and 7 T MRI data. Neuroimage 70:122–131
12. Voelker MN, Kraff O, Brenner D, Wollrab A, Stoecker T, Norris D, Ladd ME, Speck O (2015) The traveling heads: initial comparisons of multicenter data on 7 Tesla MRI systems. In: Proceedings of the 23th scientific meeting, International Society for Magnetic Resonance in Medicine, Toronto, p 3202
13. Benner T, Wisco JJ, van der Kouwe AJ, Fischl B, Vangel MG, Hochberg FH, Sorensen AG (2006) Comparison of manual and automatic section positioning of brain MR images. Radiology 239(1):246–254
14. Dou W, Speck O, Benner T, Kaufmann J, Li M, Zhong K, Walter M (2015) Automatic voxel positioning for MRS at 7 T. Magma 28(3):259–270
15. Brenner D, Tse DHY, Pracht ED, Feiweier T, Stirnberg R, Stöcker T (2014) 3DREAM—a Three-Dimensional Variant of the DREAM Sequence. In: Proceedings of the 22nd scientific meeting, International Society for Magnetic Resonance in Medicine, Milan, p 1455
16. Nehrke K, Bornert P (2012) DREAM—a novel approach for robust, ultrafast, multislice B(1) mapping. Magn Reson Med 68(5):1517–1526
17. Nehrke K, Versluis MJ, Webb A, Bornert P (2014) Volumetric B1 (+) mapping of the brain at 7T using DREAM. Magn Reson Med 71(1):246–256
18. Johst S, Wrede KH, Ladd ME, Maderwald S (2012) Time-of-flight magnetic resonance angiography at 7 T using venous saturation pulses with reduced flip angles. Invest Radiol 47(8):445–450
19. Speck O, Stadler J, Zaitsev M (2008) High resolution single-shot EPI at 7T. MAGMA 21(1–2):73–86
20. Liu S, Talagala L, Inati S, Xu Y, Chow HM, Chen G, Braun A (2015) Improvement of task-based and resting-state fMRI using GRAPPA accelerated EPI with a FLASH based reference scan. In: Proceedings of the 23th scientific meeting, International Society for Magnetic Resonance in Medicine, Toronto, p 2065
21. Jenkinson M, Beckmann CF, Behrens TE, Woolrich MW, Smith SM (2012) Fsl. Neuroimage 62(2):782–790
22. Smith SM, Jenkinson M, Woolrich MW, Beckmann CF, Behrens TE, Johansen-Berg H, Bannister PR, De Luca M, Drobnjak I, Flitney DE, Niazy RK, Saunders J, Vickers J, Zhang Y, De Stefano N, Brady JM, Matthews PM (2004) Advances in functional and structural MR image analysis and implementation as FSL. Neuroimage 23(Suppl 1):S208–S219
23. O'Brien K, Krueger G, Lazeyras F, Gruetter R, Roche A (2013) A simple method to denoise MP2RAGE. In: Proceedings of the 21th scientific meeting, International Society for Magnetic Resonance in Medicine, Salt Lake City, p 269
24. Marques JP, Kober T, Krueger G, van der Zwaag W, van de Moortele PF, Gruetter R (2009) MP2RAGE Contrast Optimization at 7T and Applications. In: Proceedings of the 17th scientific meeting, International Society for Magnetic Resonance in Medicine, Honolulu, p 2698
25. Lutkenhoff ES, Rosenberg M, Chiang J, Zhang K, Pickard JD, Owen AM, Monti MM (2014) Optimized brain extraction for pathological brains (optiBET). PLoS One 9(12):e115551
26. Zhang Y, Brady M, Smith S (2001) Segmentation of brain MR images through a hidden Markov random field model and the expectation-maximization algorithm. IEEE Trans Med Imaging 20(1):45–57

27. Patenaude B, Smith SM, Kennedy DN, Jenkinson M (2011) A Bayesian model of shape and appearance for subcortical brain segmentation. Neuroimage 56(3):907–922
28. Jenkinson M, Bannister P, Brady M, Smith S (2002) Improved optimization for the robust and accurate linear registration and motion correction of brain images. Neuroimage 17(2):825–841
29. Hurley AC, Al-Radaideh A, Bai L, Aickelin U, Coxon R, Glover P, Gowland PA (2010) Tailored RF pulse for magnetization inversion at ultrahigh field. Magn Reson Med 63(1):51–58
30. Huppertz HJ, Kroll-Seger J, Kloppel S, Ganz RE, Kassubek J (2010) Intra- and interscanner variability of automated voxel-based volumetry based on a 3D probabilistic atlas of human cerebral structures. Neuroimage 49(3):2216–2224
31. Fellhauer I, Zollner FG, Schroder J, Degen C, Kong L, Essig M, Thomann PA, Schad LR (2015) Comparison of automated brain segmentation using a brain phantom and patients with early Alzheimer's dementia or mild cognitive impairment. Psychiatry Res 233(3):299–305
32. de Boer R, Vrooman HA, Ikram MA, Vernooij MW, Breteler MM, van der Lugt A, Niessen WJ (2010) Accuracy and reproducibility study of automatic MRI brain tissue segmentation methods. Neuroimage 51(3):1047–1056
33. Jovicich J, Czanner S, Han X, Salat D, van der Kouwe A, Quinn B, Pacheco J, Albert M, Killiany R, Blacker D, Maguire P, Rosas D, Makris N, Gollub R, Dale A, Dickerson BC, Fischl B (2009) MRI-derived measurements of human subcortical, ventricular and intracranial brain volumes: reliability effects of scan sessions, acquisition sequences, data analyses, scanner upgrade, scanner vendors and field strengths. Neuroimage 46(1):177–192
34. Hennig J, Scheffler K (2001) Hyperechoes. Magn Reson Med 46(1):6–12
35. Conolly SND, Macovski A, Glover G (1988) Variable-rate selective excitation. J Magn Reson 78:440–458
36. Hutton C, Josephs O, Stadler J, Featherstone E, Reid A, Speck O, Bernarding J, Weiskopf N (2011) The impact of physiological noise correction on fMRI at 7 T. Neuroimage 57(1):101–112
37. Triantafyllou C, Hoge RD, Krueger G, Wiggins CJ, Potthast A, Wiggins GC, Wald LL (2005) Comparison of physiological noise at 1.5 T, 3 T and 7 T and optimization of fMRI acquisition parameters. Neuroimage 26(1):243–250
38. Triantafyllou C, Polimeni JR, Wald LL (2011) Physiological noise and signal-to-noise ratio in fMRI with multi-channel array coils. Neuroimage 55(2):597–606